The International Journal of Advanced Manufacturing Technology (2019) 102:705–717
https://doi.org/10.1007/s00170-018-03212-w

ORIGINAL ARTICLE

A unified prediction model of 3D surface topography in face milling considering multi-error sources

Sun Jin [1,2] · Shun Liu [1,2] · Xueping Zhang [1] · Kun Chen [1,2]

Received: 19 July 2018 / Accepted: 13 December 2018 / Published online: 5 January 2019

Abstract

Surface topography, which represents machined surface errors in 3D space, is a comprehensive way to estimate surface quality in face milling. This paper presents a unified simulation model for the prediction of 3D machined surface topography considering multiple error sources in face milling with multi-tooth cutter that has large diameter. In this model, the final machined surface topography is described with a height-encoded and position-maintained colorful surface image that consists of multi-scale errors. It is derived from a point cloud of residual surface height at each encoding contact location. The model includes the effects of milling parameters, different kinds of initial setup errors, and process static/dynamic characteristics of machine tool-workpiece-fixture system. The influences of inserts' geometric structures on roughness scale are also introduced through beam elements. A numerical algorithm is proposed to obtain the resultant point cloud based on the simulation model integrating with all the effects of influence factors. Face milling experiments are conducted to validate and investigate the proposed simulation model. Comparisons between simulated and experimental results show good agreement. And the proposed model can also be applied to investigate the topography patterns induced by multiple error sources coupled and respectively. Thus provides a comprehension methodology to predict machined surface topography and the resultant topography patterns induced by multi-error sources in face milling for its industry implementation.

Keywords 3D machined surface topography · Surface roughness · Face milling · Integrated error sources · Multi-tooth cutter · Validation

1 Introduction

Face milling with multi-tooth cutter are widely used in the manufacturing of components with complex surfaces in the automobile industry, such as in the manufacturing of engine cylinder block, engine head, crank casing, and transmission valve body [1, 2]. With the advancement of machine tool technique, more powerful machining centers are used in industry application. It can provide high cutting speed and be implemented with large cutter, thus can obtain high efficiency and prospective machining quality simultaneously. The surface quality is not only a vital indicator for the judgment of machine tool's performance in machining process but also a critical factor related to the part function in service [3, 4]. Thus, a prediction model of surface quality is important not only for designing and controlling of machine tool but also assisting manufacturing engineer to determine better milling strategies [5, 6].

Nowadays, many surface measurement techniques such as high definition metrology (HDM) and areal topography methods (ATM) have been implemented for 3D surface measurements and have provided a possibility to the estimate surface quality with surface topography of the entire machined surface [7, 8]. High density data of million points can be collected over a large surface area to represent the entire surface for post-analysis through HDM. Based on this point cloud of height, surface topography of the measured surface can be generated. It can have a comprehensive understanding of the machined surface, the machining process and the service performance with the surface topography [9, 10]. The

✉ Shun Liu
shunliu@sjtu.edu.cn

[1] State Key Laboratory of Mechanical System and Vibration, School of Mechanical Engineering, Shanghai Jiao Tong University, Shanghai 200240, China

[2] Shanghai Key Laboratory of Digital Manufacture for Thin-walled Structures, School of Mechanical Engineering, Shanghai Jiao Tong University, Shanghai 200240, China

surface topography after milling process with multi-tooth cutter having a large diameter is complex and non-homogeneous [11] due to intermittent cutting characteristic and irregular cutting trajectory of face milling [12]. Surface variation at multiple length scales, from millimeters to decimeters, can be observed in face milling with multi-tooth cutter having a large diameter for large scale components, such as engine head, engine block, and valve body [13]. Such patterns of surface topography are highly related with cutting process which involves multi-scale analysis of surface topography over a large surface area. Therefore, the machined surface should be characterized in multi-scale areas from macroscale of global area (surface variation) to microscale of local area (roughness). Traditional 2D surface quality parameters along sampling lines are not sufficient to estimate machined surface quality in these cases. A simulation model of a machined surface topography estimating the surface quality is thus highly desired.

The surface topography reflects the concave and convex of the surface height and is determined by the machining error of the actual machined surface relative to the desired ideal surface. Surface topography is produced by the relative displacement between the cutter's edge and the workpiece resulting from non-uniform material removal rate (MRR). Surface topography consists of different scales machined surface error, such as surface form error, flatness, waviness, and roughness, and can provide a comprehensive view compared with 2D surface error of single point or on a sampling line. The machined surface topography after face milling is strongly influenced by the machine tool's conditions, setup of machine tool-workpiece-fixture, parameters of milling operation, and static/dynamic characteristics of milling process. Each of them can generate different types of errors and most of researches have been conducted to study the generation of surface errors.

Geometric prediction models are widely used to simulate the generation of surface errors in milling process. Gu et al. [14] proposed a model to predict the surface flatness in face milling with considering the elastic deflection of machining system at the application points of cutting forces. State space model and differential motion vector are useful to describe the dimensional errors and quasi-static errors at form scale. Yang et al. [15, 16] proposed an equivalent fixture error model of datum error, fixture error, and machine tool path error to compensating machining variation base on differential motion vectors and state space model. The position errors and orientation errors in multi-stage machining processes are integrated with homogeneous transformation to describe the dimensional variation propagation. Paris et al. [17] and Peigné et al. [18] considered the chattering behavior of system's vibration and proposed a simulation model of milled surface shape error. Dynamic characteristics of machining system, online compensation adjustment of feed rate and trajectory location, and forced vibration in stable and unstable can have effect on the machined surface qualities [19, 20]. Belonging to these geometric prediction models of shape error generation thorough theoretical analyses, some researches focused on the effects of tool deflection on surface shape variation and the effects of wear of face mill teeth on surface roughness [21, 22]. These mentioned models are trying to simulate the generation of surface errors from different dimensional scales based on the effects of different kinds of influence factors. Through geometric prediction models and theoretical analyses, different kinds of factors can be integrated together. But most of them focus on single point error or on a plate of cutter along feed direction in the peripheral milling. Thus cannot reflect the non-uniform variation of surface topography in the face milling.

Some researchers have been conducted on simulation of 3D surface topography in milling with end miller. Lavernhe, Quinsat, and Lartigue [23, 24] studied the prediction and characterization of 3D surface topography in 5-axis milling with end miller based on N-buffer method. Zhang et al. [25] studied numerical simulation of machined surface topography in ball-end milling based on the formulation of coordinate system transformation. Omar et al. [26] introduced a prediction model of surface roughness and topography in side milling operation including a set of error sources. However, these are all about simulation of surface topography of milling with small size end miller, which cannot be applied on face milling with multi-tooth cutter which has large diameter due to intermittent cutting characteristic and irregular cutting trajectory. Nevertheless, surface topographies of face milling can be sequentially studied through experimental design based on the measurement techniques. But the error sources of machined surface in face milling cannot be effective based on the correlation analysis between experimentally measured surface topography and process variables. Therefore, a cost-effective simulation model for machined surface topography of face milling is desired and helpful for estimating surface quality and process controlling.

This paper presents a model for the simulation of surface topography including multi-scale errors after face milling. This work is focusing on face milling by multi-tooth miller with large diameter. The model integrates the effects of different kinds of error sources and influence factors on machined surface topography together through spatial transformation matrix. All the effects are transformed into the same state space of machine tool-workpiece-fixture system. The incorporated factors include the conditions of machine tool such as the spindle axis title of machine tool and the axially inclined cutting path; the characteristics of cutter such as cutter runout, cutter insert geometry, and insert runout; initial setup error of fixture layout; and the characteristics of process such as the milling parameters and static/dynamic characteristics of machine tool-workpiece-fixture system. In this model, the final machined surface topography is represented with a height-

encoded and position-maintained colorful surface image including multi-scale errors from form error to roughness. The machined surface topography is represented with the point cloud of residual surface height at each encoding contact location. Moreover, a set of face milling experiments are conducted to validate the proposed prediction model. Comparison of measured and predicted results is taken to test the accuracy of the proposed model.

2 Mathematical model of surface topography

In this section, three main coordinate systems (CSs) are established based on right-hand discipline, including the global coordinate system (GCS) and two local coordinate systems (LCSs) attached to workpiece and cutter, respectively. Simulation model of surface topography integrated with multiple error sources is established based on those established CSs. Eight kinds of influence factors are considered such as the static spindle axis tilt, the axially inclined cutter feed path, cutter runout, cutter insert geometry, insert runout, initial location error of fixture, parameters of machining process, and characteristic of system dynamic. The surface topography is encoded by the residual surface height between cutter edge and workpiece at each encoded contact location in whole machined surface of workpiece, which is finally congregated as point cloud of residual surface height of $\{z(x, y)\}$. For each insert, the real cutting edge is partitioned as small beam elements and the governing function of each element is given considering the geometry of contacted cutting blade.

2.1 Ideal formulation model of surface governing function

The involved set of CSs is established to obtain the governing functions of the machined surface topography. In Fig. 1, suppose OXYZ is the GCS in which the workpiece machined surface and the tool path are described. $O_cX_cY_cZ_c$ is a LCS attached to the cutter. $O_wX_wY_wZ_w$ is another LCS attached to workpiece.

In order to describe the machined surface topography represented with the relative displacement of cutter and workpiece, governing functions described in the CS of $O_cX_cY_cZ_c$ and CS of $O_wX_wY_wZ_w$ are transformed into the GCS of OXYZ.

2.1.1 The governing function of cutting edge

The cutting edge's effective cutting length denoted as h_D as shown in Fig. 1 is changing with the rotation angle. The surface topography model should be established considering the whole cutting edges but not only the cuter tips. To accommodate the tip's structure, the whole effective length of cutter edge is divided into beam elements. Each element is defined by two nodes, $(j, j + 1)$ for j-th beam element. The effective length of j-th node on j-th beam element of i-th cutter insert to its cutting tip can be determined by the following formula

$$r'(i,j) = \frac{j-1}{N_e} h_D(\varphi_i, \theta), (j = 1, 2, ..., N_e + 1) \quad (1)$$

where $h_D(\varphi_i, \theta)$ is the total effective cutting length of i-th cutter insert with the rotation angle $\theta = -\omega t$, where ω is the rotation angle of spindle around the clock direction. It is changing with cutter rotation angle and can be theoretically determined with the approach developed by Song [27]. N_e is the total number of sampling portions of the total effective cutting length. φ_i is the i-th insert angle, $\varphi_i = 2\pi(i-1)/5$.

Then the governing function of beam element with an effective diameter of r' is given as

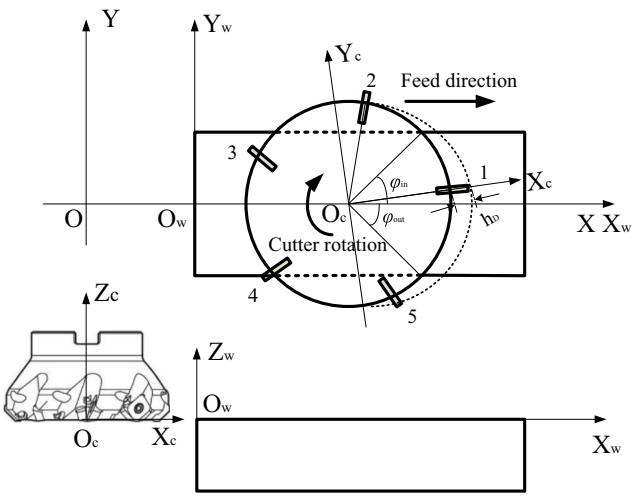

Fig. 1 Definition of coordinate systems

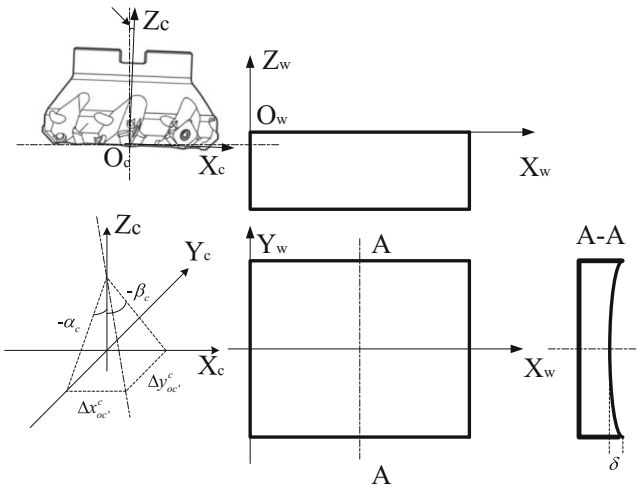

Fig. 2 Definition of spindle axis tilt and its influence on machined surface

$$P_{ci}^{o}\left(r^{'}\right)=T\left({}_{o}^{oc}P\right)R(Z_c,\theta)P_{ci}^{c}\left(r^{'}\right) \tag{2}$$

where $P_{ci}^{o}\left(r^{'}\right)$ and $P_{ci}^{c}\left(r^{'}\right)$ are the column vectors of effective beam element (coordinates of i-th cutter insert with a distance of $r^{'}$ to its cutting tip), in GCS and cutter's LCS, respectively. The column vector of effective beam element in $O_cX_cY_cZ_c$ is defined by formula of $P_{ci}^{c}(r)=\left[R'\left(r^{'}\right)\cos(\varphi_i),R'\left(r^{'}\right)\sin(\varphi_i),0,1\right]_i$, where the $R(r^{'})$ is the diameter of each effective beam element, $R(r^{'})=R-r^{'}$. R is the tool radius. The $T\left({}_{o}^{oc}P\right)$ and $R(Z_c,\theta)$ are the transformation matrix with a transformation vector from CS of $O_cX_cY_cZ_c$ to CS of OXYZ and rotational matrix with θ angle along Z_o axis between CS of $O_cX_cY_cZ_c$ and CS of OXYZ, respectively.

2.1.2 The governing function of workpiece

The origin point of workpiece CS is assuming on the OX axis with a distance of tool radius. Then an arbitrary point on workpiece with coordinates of $P_w^o=\left[x_w^o,y_w^o,z_w^o,1\right]^T$ can be expressed as

$$P_w^o=T\left({}_{o}^{ow}P\right)P_w^w \tag{3}$$

where $T\left({}_{o}^{ow}P\right)$ is the transformation matrix of workpiece CS of $O_wX_wY_wZ_w$ to the GCS of OXYZ with a displacement vector ${}_{o}^{ow}P$. ${}_{o}^{ow}P$ is vector from OXYZ origin to $O_wX_wY_wZ_w$ origin.

2.1.3 Formulation of surface topography

The surface topography is simulated as point cloud of surface height that is represented as $\{z(x,y)\}$. The surface point cloud can be used to describe the surface texture by a height-encoded and position-maintained colorful surface image. It is the foundation to analyze machined surface quality, such as form, waviness, and roughness.

Based on the results of previous works [12, 26, 28, 29], the machined surface error is the result of various factors that generate the variation of actual material removal during milling process. For each cutting immersion point, the actual geometric dimension of machined surface after milling is determined by the Z-axial instantaneous relative displacement of intersection between i-th effective cutting tooth and workpiece.

At each time step of t in milling process, the height of cutting point is determined by the relative distance between cutter insert and workpiece at the same point (x, y). At every time step, the position of cutting insert can be determined by

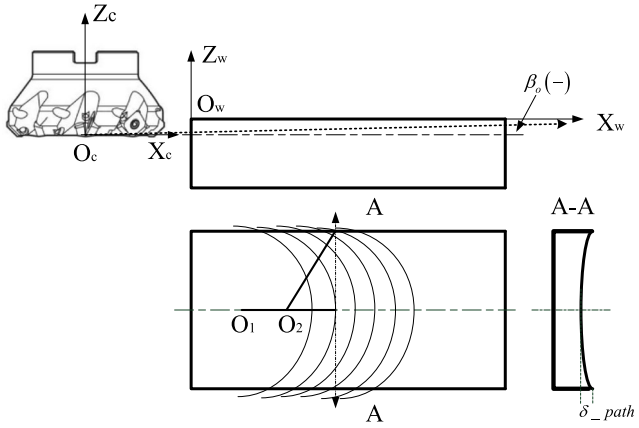

Fig. 3 Definition of axially inclined cutter feed path and its influence on machined surface

Eq. (2). And the local coordinate of contact point of cutting insert on workpiece at time step of t can be calculated by Eq. (3). Then the surface height of j-th node on j-th beam element of i-th cutter insert can be expressed as

$$z(x,y,t)_i^j=z_{w0}^o\left(x_w^o,y_w^o,t\right)_i^j-\left[z_w^o\left(x_w^o,y_w^o,t\right)_i^j-z_c^o\left(x_c^o,y_c^o,t\right)_i^j\right] \tag{4}$$

where $x|_t=x_c^o|_t=x_w^o|_t$ and $y|_t=y_c^o|_t=y_w^o|_t$ are the coordinates of contact point between cutter (j-th node) and workpiece at time step of t. z_{w0}^o is the nominal machining surface on workpiece.

For each cutting instant, the location (x, y) of the immersion point is calculated by the Eq. (2) and Eq. (3) in the space domains of cutter and workpiece, respectively. It involves the calculation of the locations in both CSs of cutter and workpiece, and the unified transformation of these two locations from these two LCSs into the GCS. Thereafter, the Z-axial displacements of cutter and workpiece corresponding to the immersion point are determined. Eventually, the surface error is calculated in Eq. (4).

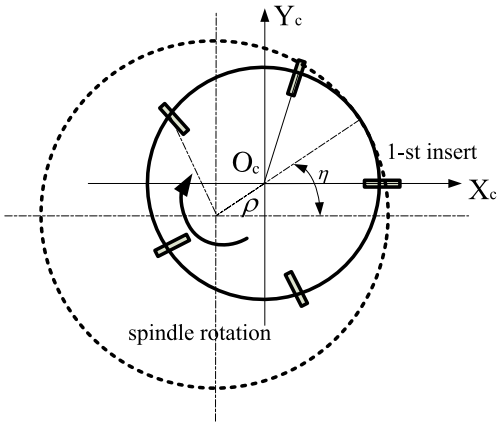

Fig. 4 The definition of cutter runout

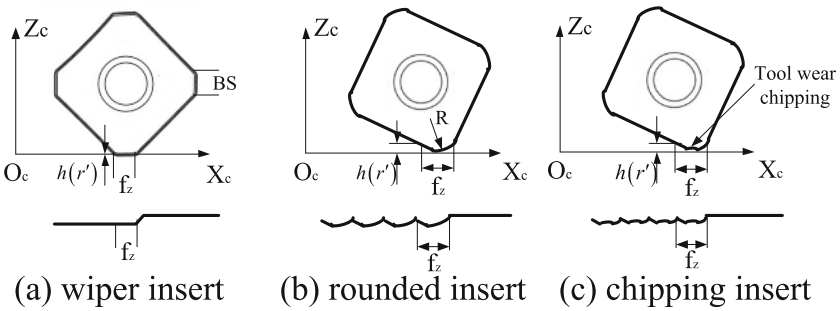

Fig. 5 Definition of geometry of cutter insert and its influence on machined surface

2.2 Influences of sources of machining errors

During face milling process, there are several errors from the machine tool, spindle axis, workpiece, fixture and machining parameters, and others that can deteriorate or improve the machined surface quality. In this paper, eight kinds of error sources are considered to formulate the surface topography model, and the model presented in Section 2.1 is then combined with these sources of errors.

2.2.1 Static spindle axis tilt

Static spindle axis tilt is induced by the initial setup error and also the instant tilt caused by the moment of cutting force along axial and feed direction. The moment-induced cutter-spindle tilt is proportional to the instant cutting force [13]. As shown in Fig. 2, spindle axis tilt is described by three parameters: the pitch angle around *y*-axis, roll angle around *x*-axis, and a displacement vector.

With spindle axis tilt, the cutter will have a deviation compared with the cutter LCS of $O_cX_cY_cZ_c$ at ideal condition. Assuming the LCS of tilted cutter is $O_c{}'X_c{}'Y_c{}'Z_c{}'$, the surface model in Eq. (2) can be rewritten as

$$P_{ci}^{o}\left(r'\right) = T\left({}_{o}^{oc}P\right)T\left({}_{c}^{oc'}P'\right)R(X_c,\alpha_c)R(Y_c,\beta_c)R(Z_{c'},\theta)P_{ci}^{c'}\left(r'\right) \quad (5)$$

where $T\left({}_{c}^{oc'}P'\right)$ is the transformation matrix from tilted CS of $O_c{}'X_c{}'Y_c{}'Z_c{}'$ to ideal CS of $O_cX_cY_cZ_c$ with a displacement vector ${}_{c}^{oc'}P' = \left[\Delta x_{oc'}^{c}, \Delta y_{oc'}^{c}, \Delta z_{oc'}^{c}, 1\right]^t$. $R(X_c, \alpha_c)$, $R(Y_c, \beta_c)$, and $R(Z_{c'}, \theta)$ are the rotation matrix around axis O_cX_c, O_cY_c, and $O_c{}'Z_c{}'$ with rotation angle of α_c, β_c, and θ, respectively.

2.2.2 Axially inclined cutter feed path

The axially inclined cutter feed path can be described as a real cutting plate with a pitch angle β_o to the ideal cutting plate as shown in Fig. 3. The presence of cutter path inclination causes a varying cutting depth distribution which results in an uneven cutting force distribution along feed direction. Similarly with the static spindle axis tilt, the axially inclined tool feed path could avoid back-cutting.

Then the surface governing formula integrated with axially inclined cutter feed path can be rewritten as

$$P_{ci}^{o}\left(r'\right) = T\left({}_{o}^{o'}P\right)T\left({}_{o'}^{oc}P^{o'}\right)R(Z_c,\theta)P_{ci}^{c}\left(r'\right) \quad (6)$$

where $T\left({}_{o'}^{oc}P^{o'}\right)$ is the transformation matrix of cutter origin along cutting path with a displacement vector ${}_{o'}^{oc}P^{o'} = [ft, 0, ft\tan(\beta_o), 1]^t$.

2.2.3 Cutter runout

The cutter runout is defined by the eccentricity between the *Z*-axial cutter's geometrical center and the *Z*-axial rotation center. It will change the real cutting radius that results in the varying undeformed-chip width. Two parameters are used to describe the cutter runout as shown in Fig. 4, the runout vector

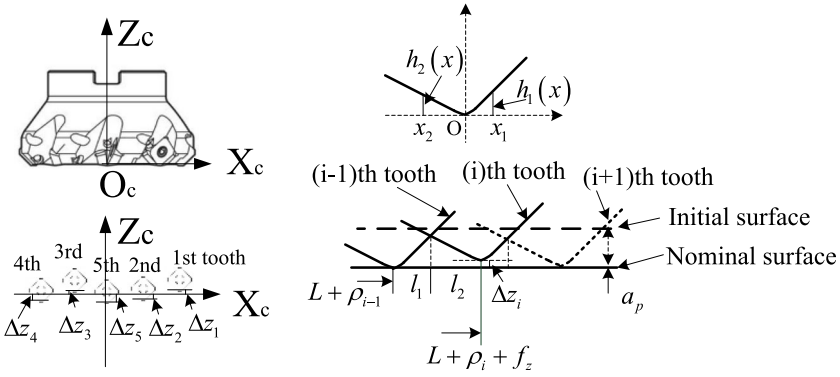

Fig. 6 Definition of insert runout and its influence on machined surface

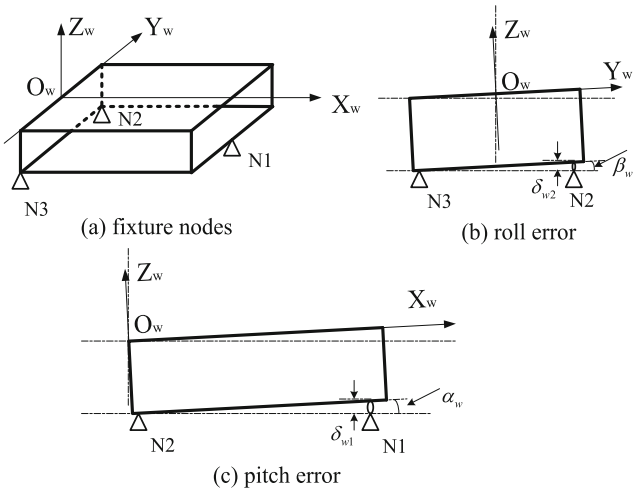

Fig. 7 Definition of initial fixture location error and its influence on machined surface

of cutter center point (ρ, η) containing runout distance of ρ and runout angle of η.

Then the cutter inserts' position is transformed from eccentric LCS of cutter with eccentricity to ideal LCS of cutter are rewritten as

$$P_{ci}^{o}\left(r^{'}\right) = T\left({}_{o}^{oc}P\right)R(Z_c,\theta)T\left({}_{c'}^{oc''}P^{c'''}\right)P_{ci}^{c''}(r) \tag{7}$$

where $T\left({}_{c'}^{oc''}P^{c'''}\right)$ is the transformation matrix from eccentric CS of O_c-X_c-Y_c-Z_c to ideal CS of O_c-X_c-Y_c-Z_c with a displacement vector ${}_{c'}^{oc''}P^{c'''} = [\rho\cos\eta, \rho\sin\eta, 0, 1]^t$.

As the previous work by Yang [28], the cutter runout can be identified as the difference value of the cutter rotary eccentricities which are measured by laser sensor under low-speed rotation status and high-speed rotation status without machining, respectively.

2.2.4 Cutter inserts geometry

Cutting edges are produced by the contact cutting blade with a width along the cutter radius. The cutter insert geometry especially the blade geometry will affect the Z-axial residual height along the cutting edges in radial direction [30]. Tool wear changes the insert geometry during milling process in practical application, which will be resulted in the microscale roughness of machined surface. The geometry of tool wear can be characterized by the geometrical model proposed by Pimenov [22]. Several kinds of general geometries of cutter insert are shown in Fig. 5.

The initial depth of cutter tips on Z-axial direction is changing along radial position according to the geometry of cutter insert. The initial depth $h(r^{'})$ is determined by the geometry and the radial position, and it will affect the residual cutting materials along the effective cutting length. With beam elements, the effects of microscale roughness corresponding to the changing geometry of cutter blade can be partitioned modeled. The governing function of beam element on cutter insert can be renewed as

$$P_{ci}^{o}\left(r^{'}\right) = T\left({}_{o}^{oc}P\right)R(Z_c,\theta)P_{ci}^{c}\left(r^{'},h\left(r^{'}\right)\right) \tag{8}$$

where $P_{ci}^{c}\left(r^{'},h\left(r^{'}\right)\right) = \left[R^{'}\left(r^{'}\right)\cos(\varphi_i), R^{'}\left(r^{'}\right)\sin(\varphi_i), h\left(r^{'}\right), 1\right]_i^t$ and $h(r^{'})$ is the height of cutter blade in LCS of cutter at the point with a distance $r^{'}$ to the edge of cutter tip.

2.2.5 Insert runout

The insert runout is defined by the position errors of i-th insert compared with the ideal insert position, which is mainly caused by setup error and manufacturing error of insert. There are two parameters to describe the insert pre-set induced insert runout, Z-axial runout error of Δz_i and radial runout error of ρ_i. They can be measured by tool presetting and measuring machine based on CCD imaging in static status.

For each element of insert as shown in Fig. 6, the real initial height of cutting beam element on cutter blade with initial insert runout, $h(r^{'})$, is determined by the combination of trajectories of two neighbor inserts. The height of cutting beam element is divided into two parts, ahead and behind the cutting tip or the blade center of o. Then the surface governing formula integrated with insert runout is refreshed as

$$P_{ci}^{o}\left(r^{'}\right) = T\left({}_{o}^{oc}P\right)R(Z_c,\theta)P_{ci}^{c}\left(r^{'},\rho_i,\Delta z_i\right) \tag{9}$$

where $P_{ci}^{c} = \left[\left(R^{'}\left(r^{'}\right)+\rho_i\right)\cos(\varphi_i), \left(R^{'}\left(r^{'}\right)+\rho_i\right)\sin(\varphi_i), \Delta z_i\left(r^{'}\right), 1\right]_i^t$ and $\Delta z_i(r^{'})$ is the Z-axial runout to the nominal machining surface of element with a distance of $r^{'}$. It can be determined by the geometry of insert and initial Z-axial runout error of tip that $\Delta z_i(r^{'}) = \Delta z_i + h(r^{'})$.

2.2.6 Initial location error of fixture

Generally, the workpieces are installed on standard fixture. Because of manufacturing error or installation errors of fixture in practical manufacturing, the real location of workpiece will deviate from the ideal place, and so it is with the nominal machining surface. The general description of the influence of fixture error on machined surface is shown in Fig. 7.

The error plane of workpiece described by deviation angles of (α_w, β_w, γ_w) forms the ideal plane of fixture datum and deviation of origin point of $(\Delta x_{w0}, \Delta y_{w0}, \Delta z_{w0})^T$. Only the *Z*-axial direction errors are concerned to determine the practical nominal cutting surface. Then the surface governing formula integrated with location error of fixture can be rewritten as

$$P_w^o = T\left({}_o^{ow}P\right)T\left({}_w^{ow'}P\right)R(X_w, \alpha_w)R(Y_w, \beta_w)P_w^{w'} \tag{10}$$

where $T\left({}_w^{ow'}P\right)$ is the transformation matrix of workpiece tilted CS of O_w-X_w-Y_w-Z_w- to the ideal LCS of $O_wX_wY_wZ_w$ with vector ${}_w^{ow'}P$. ${}_w^{ow'}P$ is the vector from $O_wX_wY_wZ_w$ origin to O_w-X_w-Y_w-Z_w- origin. $R(X_w, \alpha_w)$ and $R(Y_w, \beta_w)$ are the rotation matrix around axis O_wX_w and O_wY_w with rotation angle α_w and β_w, respectively.

2.2.7 Parameters of machining process

The parameters of machining process, including the spindle speed, the feed rate, and the depth of cut, have direct or indirect influence on the machined surface topography. For example, the feed rate is directly related with the width of undeformed-chip and then related with the machined surface topography grooves. Whereas, the spindle speed, depth of cut, and feed rate, these parameters will determine the cutting force combining together, thus to influence the actual material remove and the surface topography indirectly.

2.2.8 Characteristic of system dynamic

In this study, only the motions in *Z*-axial direction of workpiece and cutter insert caused by cutting force variation are considered to generate the machined surface errors. Consequently, the effects of forced vibration on the surface roughness are taken into account, while the effects of regenerative chatter caused by the self-excited vibration are neglected [12, 28]. The dynamic movement of machining system which consists of machine tool and workpiece can be represented by an equivalent of a single degree of freedom spring-mass-damper system in the *Z*-axial direction both for the machine tool and workpiece, respectively. Based on the modal differential equations (MDEs) of machining system [12], the *Z*-axial relative displacements between the cutter insert and workpiece can be calculated by MDEs under stable cutting condition with updating the instantaneous vibration displacement of milling system caused by cutting force variation. Then at t moment, the *Z*-axial relative displacement $z_{DR}(t)$ between the cutting insert and workpiece can be updated as

$$z_{DR}(t) = \delta_c - \delta_w \tag{11}$$

where δ_c and δ_w are respectively the instantaneous vibration displacement of the cutter insert and of the workpiece along the *Z*-axial direction caused by the cutting force.

Based on the previous work by Shi [12], three steps are needed to obtain the *Z*-axial relative displacements induced by the force vibration between the cutting insert and workpiece: (1) determine the modal parameters of face milling system in the MDEs based on modal impact experiments [31], (2) acquire the *Z*-axial cutting force through force measurement in face milling experiment [32], (3) obtain the instantaneous vibration displacements of cutter and workpiece by solving the MDEs according to the measured modal parameters and *Z*-axial cutting force.

2.3 Unified model integrated with error sources

By a comprehensive description of all the error sources, the practical governing functions of cutter, workpiece, and the machined surface topography can be obtained. The model of cutting edges unified with sources of error of j-th node on j-th beam element of i-th cutter insert having an effective cutting length of $r'(i,j)$ can be expressed as the following formula

$$P_{ci}^o\left(r'\right) = T\left({}_o^{o'}P\right) \times T\left({}_{o'}^{oc}P^{o'}\right) \times T\left({}_c^{oc'}P^{'}\right)R(X_c, \alpha_c)R(Y_c, \beta_c) \times R(Z_{c'}, \theta) \times T\left({}_{c'}^{oc''}P^{c'''}\right) \times P_{cr}^c\left(r', \rho_i, h\left(r'\right), \Delta z_i\right) \tag{12}$$

$$= \begin{bmatrix} M_r\cos(\beta_c) + \mathrm{Q}_r\sin(\beta_c) + \Delta x_{oc'}^c + ft, \\ M_r\sin(\alpha_c)\sin(\beta_c) + N_r\cos(\alpha_c) - \mathrm{Q}_r\sin(\alpha_c)\cos(\beta_c) + \Delta y_{oc'}^c, \\ -M_r\cos(\alpha_c)\sin(\beta_c) + N_r\sin(\alpha_c) + \mathrm{Q}_r\cos(\alpha_c)\cos(\beta_c) + \Delta z_{oc'}^c - a_p - ft\tan(\beta_o), \\ 1 \end{bmatrix}_i$$

where

$$\begin{bmatrix} M_r \\ N_r \\ \mathrm{Q}_r \\ 1 \end{bmatrix}_i = \begin{bmatrix} \left(R'\left(r'\right)+\rho_i\right)\cos(\varphi_i+\theta)+\rho\cos(\eta+\theta) \\ \left(R'\left(r'\right)+\rho_i\right)\sin(\varphi_i+\theta)+\rho\sin(\eta+\theta) \\ h\left(r'\right)+\Delta z_i \\ 1 \end{bmatrix}_i$$

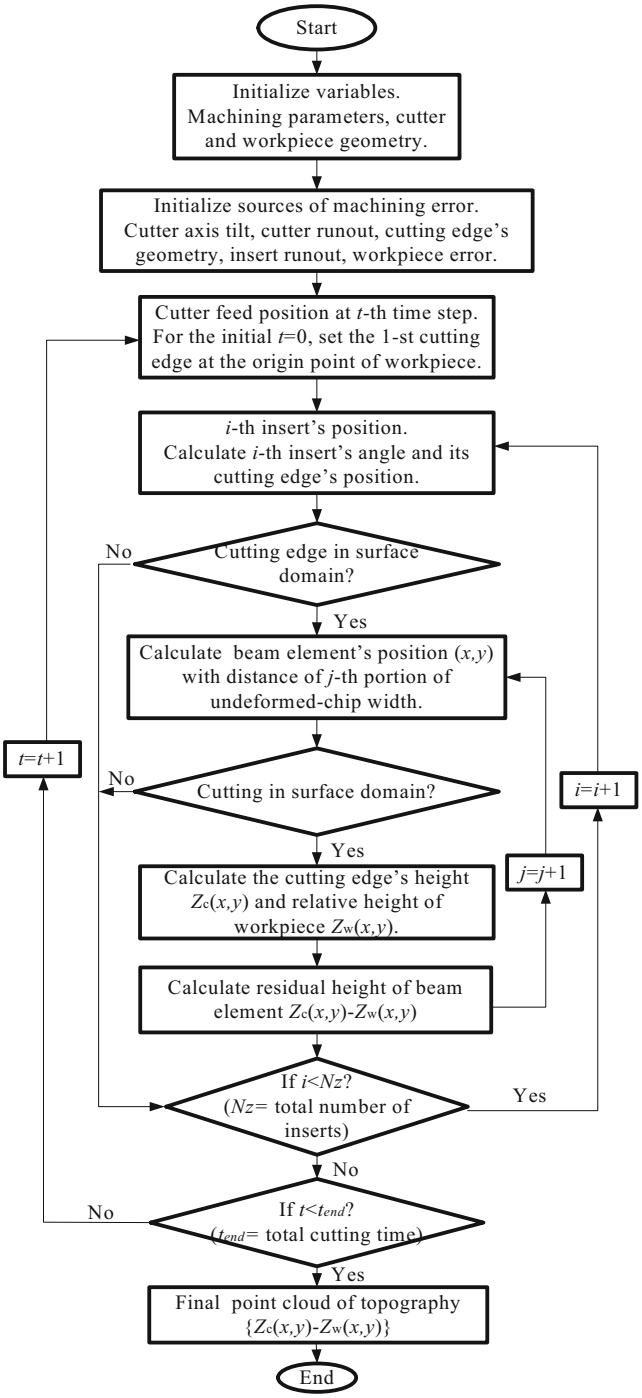

Fig. 8 The simulation algorithm of machined surface topography

After the determination of location of cutter edges and workpiece, the formula of surface topography can be finally obtained as

$$z(x,y) = z^o_{w0}\left(x^o_w, y^o_w\right) - \left(z^o_w\left(x^o_w, y^o_w\right) - z^o_c\left(x^o_c, y^o_c\right)\right) + z_{DR}(t) \quad (13)$$

3 Algorithm of simulation and post-process

This section will summarize the solution procedure for face milling simulation in Section 2 with the flow chart as shown in Fig. 8.

The flow chart of principle and complete procedures is explained briefly in the following. For each cutting step, the cutting trajectories of cutter tips are evenly discretized as coordinate points both in cutter angular step and feed step. For each insert in the cutting surface domain, the cutting width is partitioned as small beam elements, thus it can be used to reflect the geometry of cutting insert. Each small beam element is proportional to the feed rate per tooth. That is to say, the total number of small beam elements is varying to the real undeformed-chip thickness. For each small beam element of cutting edges in cutting area, both the height of cutting edge and the height of cutting point in workpiece can be calculated according to the element's coordinates (x, y) and so it is with the final residual height of cutting point. Then the same procedure is repeated to calculate the residual height distribution for those beam elements in the instantaneous cutting edge until the j-th beam element is out of the real undeformed-chip thickness. The next cutting step is carried until the residual heights of all the nodal points on the total inserts are obtained. The same procedure is repeated for the nest cutting step until the cutter leaves the cutting area. At last, a point cloud of surface residual height can be obtained to describe the machined surface.

A post-procedure for the point cloud of surface residual height is proposed in order to obtain a height-encoded and position-maintained colorful surface image [10]. The post-procedure is carried out based on the software of Matlab R2014a. Usually, three steps are needed such as leveling operation, grid generation, and colorful converting. The first step is obtaining a point cloud on the nominal machining surface. A least square plane is fitted to represent the nominal machining surface. The second step is to generate a regular grid of machined surface. A continuous surface can be interpolated using coordinates of original leveled point cloud by Delaunay triangulation. Then the column data of point cloud is transformed into a panel data of interpolated surface. Then the last step is to convert the interpolated panel data into colorful image. Each element of the panel data is encoded into color as a pixel of the image. After the post-procedure, the residual

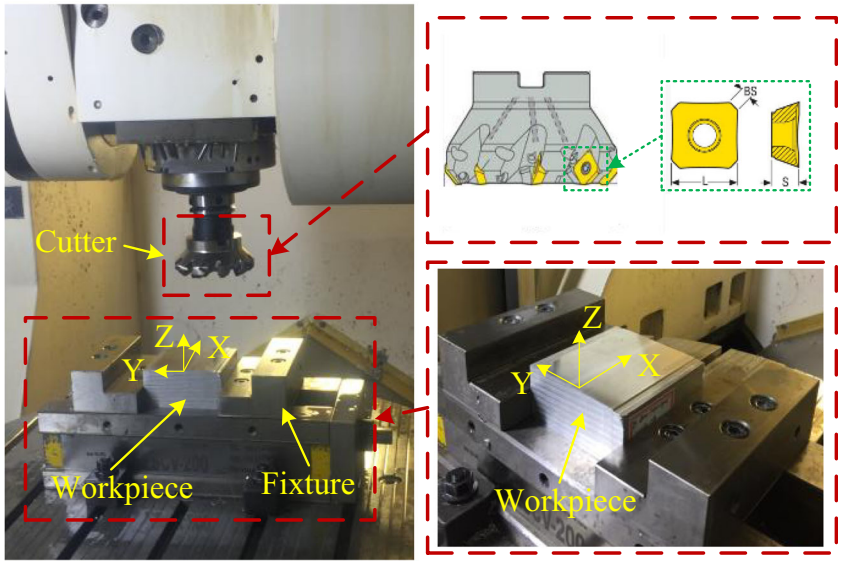

Fig. 9 Experimental setups of face milling

heights are indicated by different colors and then a colorful map of the surface topography can be derived. Based on it, different kinds of surface parameters can be calculated.

4 Case study

Face milling experiments were conducted on a five-axis machining center (DMG HSC-75) to test the proposed numerical methodology. The experimental setups are shown in Fig. 9. The workpiece was directly clamped with a vise through the vertical direction of feed in the milling tests. A case aluminum fixture was mounted between workpiece and vise. The material of workpiece is 5054 aluminum alloy and the dimensions are 100 mm × 100 mm in size and 60 mm in thickness. The effective machined area is 100 mm × 80 mm on the top of workpiece as shown in Fig. 10.

The milling tool is a 100 mm diameter face mill with 10 inserts while only 5 interval inserts were applied during the experiments. The axial runout and radial runout for each cutting tips were measured. The parameters of face milling cutter and inserts are given in Table 1.

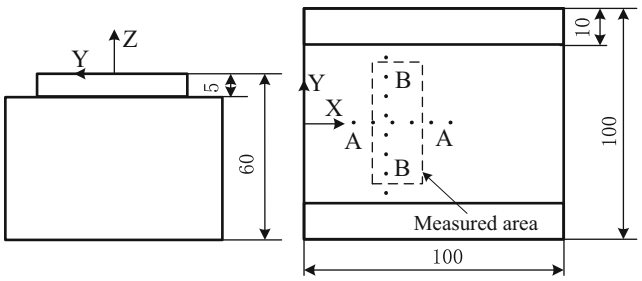

Fig. 10 The geometry of workpiece and the sampling measured area (unit: mm)

Two different tests were taken with different feed rates for investigating the model accuracy: Test I 0.3 mm/tooth and Test II 0.5 mm/tooth, respectively. And the spindle speed is 1000 r/min. The depth of cut is 0.5 mm. All the machining operations were performed on dry condition. And for each test, the face mill milled through the middle of the workpiece to generate the machined surface with different spindle titled induced by different cutting forces.

The detail process parameters of face milling operations and the parameters of error sources of machined surface were identified during this set of experiments and then used in the simulations with the same values. The static tilting angle of spindle axis can be estimated using several tool marks of measured surface texture based on the method proposed by Nguyen [13]. The surface texture was measured by surface optical profiler (KEYENCE KS-1100). Only the static spindle axis tilt angle around *Y*-axis was considered in this study, it can generate the *Z*-axial errors of machined surface. Whereas the spindle tilting angle around *X*-axis and the displacement vector of cutting center, which mainly generated the runout of cutting trajectory in cutting plane, were assumed keeping

Table 1 Parameters of the face cutter and inserts

Parameters	
Radius of face cutter (mm)	100
Number of effective teeth	5
Approach angle (°)	45
Radial rake angle (°)	− 5.0
Axial rake angle (°)	20.0
Wiper edge length (mm)	1.5
Cutting edge length (mm)	12.7
Insert thickness (mm)	4.8

small and ignored in face milling. Consequently, the identified values of spindle axis tilt angles used in two cases were 6.9×10^{-3}(°) of spindle tilted in test I and 9.2×10^{-3}(°) of spindle tilted in test II. The dynamic spindle runouts (defined as cutter runout in Fig. 4) were recognized as very small during face milling on machining center and the values in this set of experiments are zeros. The insert runout of five effective teeth cutter installed in face milling experiment was measured by tool presetting and measuring machine (ZOLLER Tool Inspection-Redomatic 600) in static status before experiments. They were calibrated based on the measured surface texture of machined surface after face milling. The final measured axial runout of each insert is recognized as 8.6, − 3.4, − 4.4, − 5.4, and − 4.6 μm and the radial runout is − 9.6, 3.6, − 23.4, − 0.4, and 10.6 μm, respectively.

After face milling process, the machined surfaces in the two tests were measured by CMM-Leitz PMM-Xi to get the point cloud of the residual surface heights of machined surfaces. The measurement areas were set as 4.5 mm × 72 mm with different scanning steps, step of 0.12 mm for Test I and step of 0.15 mm for Test II, respectively. The measured point clouds of machined surfaces were then processed with MATLAB R2014a to get the topographies. Besides, two sampling lines were extracting from the point cloud to reflect the variations along center line (A-A) in feed direction and along the perpendicular line (B-B) in cross sections, respectively.

During face milling process, the cutting forces are changing with the material removal rate which is differing with cutting positions and rotation angles. The cutting forces in the two tests were different because of different feed rates. The dynamic axial displacement between workpiece and cutter were considered in the case studies. In this study, the representative instantaneous dynamic *Z*-axial displacement of case I is simulated as shown in following Fig. 11.

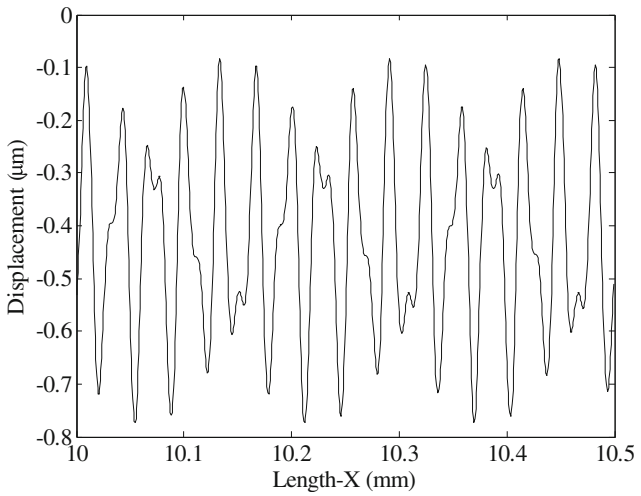

Fig. 11 Simulated dynamic *Z*-axial displacement between workpiece and cutter

The predicted topographies are generated based on the proposed model with the same parameters which are applied in the machining experiments. And, because several teeth contribute to generate the machined surfaces, the surface topographies are simulated considering the spindle tilt reduced under the cutting force, the axial runout and radial runout errors of the face cutter. After that, they are compared with the measured results. The surface topographies obtained experimentally and numerically are illustrated in Fig. 12 for the two cases with different milling feed rates.

And also the surface variations along the center line in *X*-direction and cross-section in *Y*-direction are demonstrated in Fig. 13 and Fig. 14, respectively.

It can be seen from Fig. 12a and b in case I and Fig. 12c and d in case II that the contours of the simulated and the measured surface are in agreement. Surface topographies generated in face milling by cutter with large diameter consists of grooves. And the width of grooves generated with feed rate of 0.3 mm/tooth is larger than that of feed rate of 0.5 mm/tooth. The grooves are narrower and narrower along *Y*-direction from center to the edges. The range of surface errors for the machined surface generated with feed rate of 0.3 mm/tooth is larger than that of feed rate of 0.5 mm/tooth. For the face milling by multi-tooth cutter with wiper, the view of topography with grooves is mainly affected by the feed rate on the width of grooves. While the height of surface roughness or the profiles are affected much more by the axial and radial runout than the cutting parameters of feed rate.

In Fig. 13, the predicted values are highly consisted with the measured. In Fig. 13b and Fig. 14b, when compared to experimental results, the simulated surface profile along perpendicular sampling line (B-B) is found to be in good agreement with the measured ones. The difference between the predicted values and the measured values in Fig. 14b in the center areas may come from the non-uniform along feed direction that the profiles may produce with different inserts with different axial runout. Moreover, the difference of profiles in Fig. 14a is larger than that of in Fig. 13a, it may come due to the larger dynamic displacement generating by the larger cutting forces and larger feed rate. From above results, it can be concluded that the surface topography model is capable for the simulation of machined surface topography generated in face milling with multi-tooth cutter.

Surface parameters of the surface topographies shown in Fig. 12 are listed in Table 2 for comparison. Among the arithmetic mean surface roughness S_a and root mean square surface roughness S_q based on statistical evaluation of height distribution, energy and entropy in four directions (0°, 45°, 90°, 135°) based on gray level co-occurrence matrix theory are also studied. They can reflect the local distribution patterns of different surfaces [8, 10]. In the case I, the parameters in simulation and experimental show good agreement with each other. The errors relative to the measured values of S_a, S_q, and entropy are 8.28%,

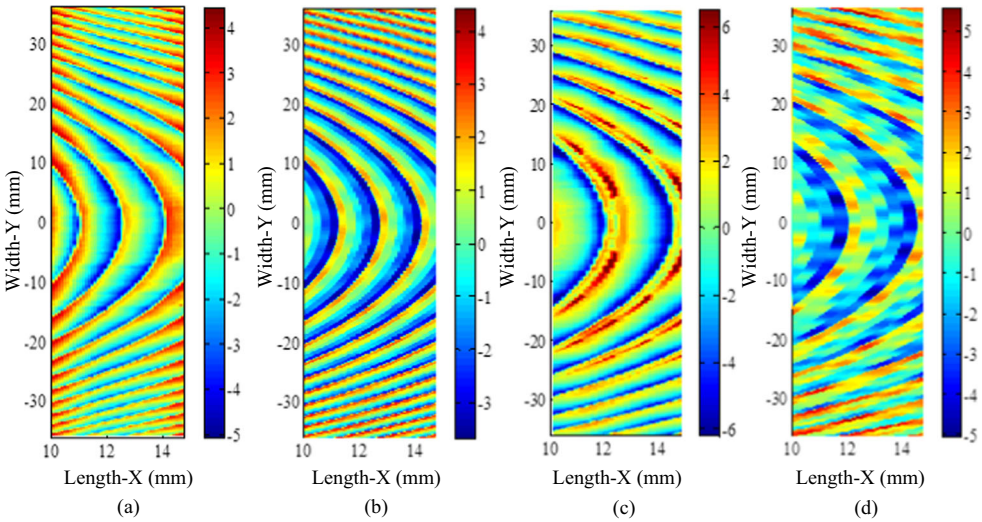

Fig. 12 Measured and simulated machined surface topographies: **a** measured topography in Test I (f_z=0.3 mm/tooth); **b** simulated topography in Test I (f_z=0.3 mm/tooth); **c** measured topography in Test II (f_z=0.5 mm/tooth); **d** simulated topography in Test II (f_z=0.5 mm/tooth)

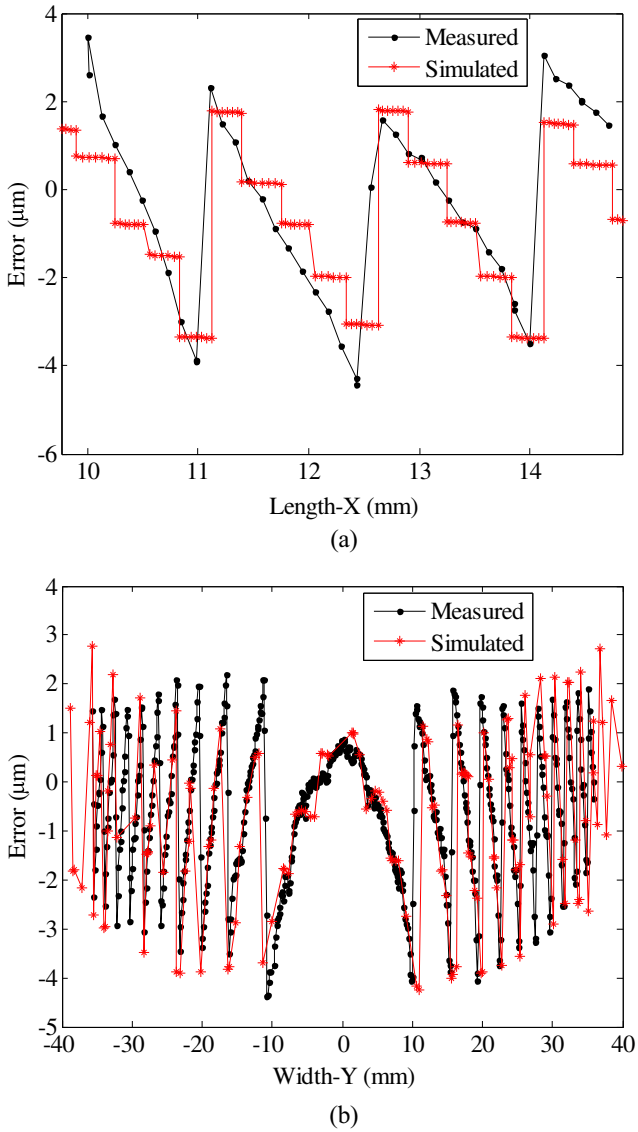

Fig. 13 Comparison between measured and simulated surface profiles in Test I (f_z=0.3 mm/tooth) along sampling lines: **a** A-A; **b** B-B

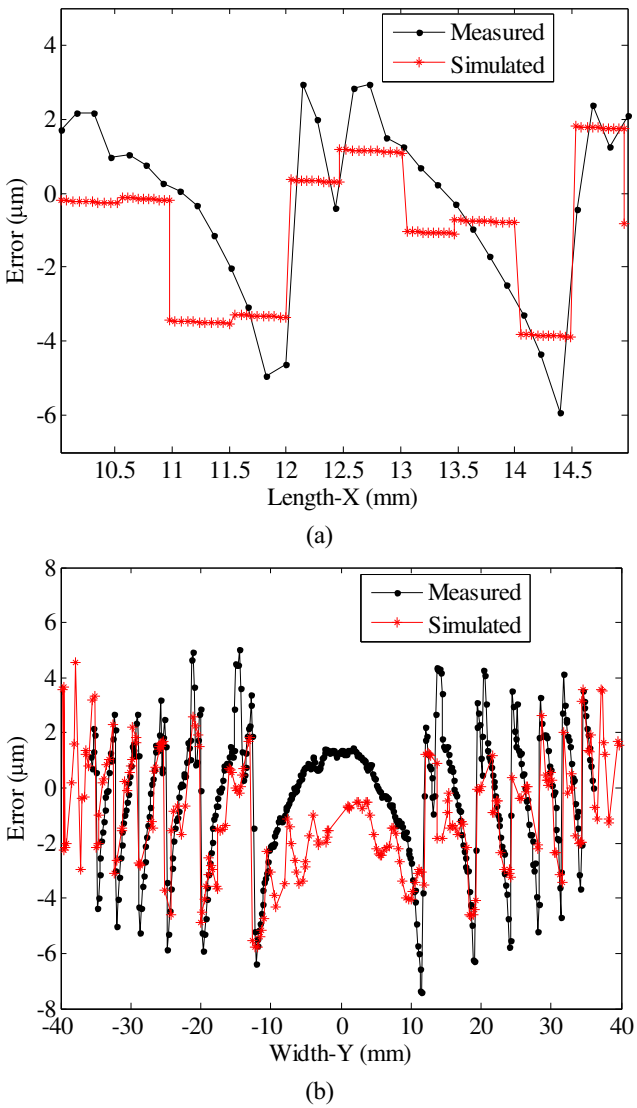

Fig. 14 Comparison between measured and simulated surface profiles of Test II (f_z=0.5 mm/tooth) along sampling lines: **a** A-A; **b** B-B

Table 2 Statistical comparison of surface topography parameters

Parameter	Test I		Test II	
	Measured	Simulated	Measured	Simulated
S_a (μm)	1.45	1.57	2.17	1.72
S_q (μm)	1.76	1.85	2.86	2.09
Energy mean	0.0029	0.0022	0.0084	0.0035
Energy st. d	0.0008	0.0005	0.0037	0.0026
Entropy mean	6.13	6.37	5.27	6.17
Entropy st. d	0.161	0.156	0.259	0.304

5.11%, and 4.03%, respectively, which are smaller than that shown in Ref. [28]. The deviation value of energy in case I is 0.0007 which is very small. The comparison results show the high accuracy of the proposed simulation method. Although the surface topography and surface parameters show a good level of coherence in case I, there are some deviations between simulated and measured surface parameters in case II which is conducted with a larger feed rate. Frankly, the cutting heat and regenerative effect caused by the self-excited chatter are neglected in the simulation which could have large influence on surface parameters in face milling with large feed rate. Therefore, the difference between the measured and simulated surface parameters is relatively large in face milling with large cutter and large feed rate. Besides, further investigations are needed to investigate the regenerative effect of cutting force and cutting heat on surface parameters.

5 Conclusions

This paper focused on the prediction of machined surface topography in face milling with multi-tooth cutter which has large value of diameter and cutting wipers on the inserts. A unified geometric methodology for the prediction was proposed and validated with face milling tests.

The prediction model can generate point cloud to simulate the topography of machined surface resulting from the face milling process using a multi-tooth cutter. The unified model was established by considering the geometry of cutter inserts, the parameters of machining process, machine-tool-workpiece dynamics, and integrating together with several sources of errors including the spindle axis tilted error, cutting path inclined error, cutter runout both in axial and radial directions, initial location error of fixture. The verification results showed that the proposed model could be capable for the simulation of machined surface topography.

Tests can be furtherly taken to study the model's sensitivity to several sources of errors based on the unified model. The different patterns of topographies resulted from the coupling error sources can be investigated.

Funding information This research is supported by the National Natural Science Foundation of China under project No. 51535007, the National Natural Science Foundation of China under project No. 51675339, and Shanghai GM PTME Company under project No. PS23005233.

References

1. Nguyen HT, Wang H, Tai BL, Ren J, Jack Hu S, Shih A (2016) High-definition metrology enabled surface variation control by cutting load balancing. J Manuf Sci Eng-Trans ASME 138:21010
2. Wang M, Shao YP, Du SC, Xi LF (2015) A diffusion filter for discontinuous surface measured by high definition metrology. Int J Precis Eng Manuf 16:2057–2062
3. Franco P, Estrems M, Faura F (2008) A study of back cutting surface finish from tool errors and machine tool deviations during face milling. Int J Mach Tools Manuf 48:112–123
4. Zhang C, Zhang H, Li Y, Zhou L (2015) Modeling and on-line simulation of surface topography considering tool wear in multi-axis milling process. Int J Adv Manuf Technol 77:735–749
5. Ghosh G, Mandal P, Mondal SC (2017) Modeling and optimization of surface roughness in keyway milling using ANN, genetic algorithm, and particle swarm optimization. Int J Adv Manuf Technol 2: 1–20
6. Liu S, Jin S, Zhang X, Chen K, Wang L, Zhao H (2018) Optimization of 3D surface roughness induced by milling operation for adhesive-sealing. Procedia CIRP 71:279–284
7. Suriano S, Wang H, Shao C, Hu SJ, Sekhar P (2015) Progressive measurement and monitoring for multi-resolution data in surface manufacturing considering spatial and cross correlations. IIE Trans 47:1033–1052
8. Wang M, Xi L, Du S (2014) 3D surface form error evaluation using high definition metrology. Precis Eng 38:230–236
9. Deltombe R, Bigerelle M, Jourani A (2015) Analysis of the effects of different machining processes on sealing using multiscale topography. Surf Topogr-Metrol Prop 4:15003
10. Liu S, Jin S, Zhang XP, Wang LX, Mei BF, Hu B (2017) Controlling topography of machined surface for adhesive-sealing. Proceedings of the ASME 2017 12th International Manufacturing Science and Engineering Conference, Los Angeles, CA, USA
11. Nguyen HT, Wang H, Hu SJ (2013) Characterization of cutting force induced surface shape variation in face milling using high-definition metrology. J Manuf Sci Eng-Trans ASME 135:41014
12. Shi Z, Liu L, Liu Z (2015) Influence of dynamic effects on surface roughness for face milling process. Int J Adv Manuf Technol 80: 1823–1831
13. Nguyen HT, Wang H, Hu SJ (2014) Modeling cutter tilt and cutter-spindle stiffness for machine condition monitoring in face milling using high-definition surface metrology. Int J Adv Manuf Technol 70:1323–1335
14. Gu F, Melkote SN, Kapoor SG, Devor RE (1997) A model for the prediction of surface flatness in face milling. J Manuf Sci Eng-Trans ASME 119:476–484
15. Yang F, Jin S, Li Z (2016) A comprehensive study of linear variation propagation modeling methods for multistage machining processes. Int J Adv Manuf Technol 90:2139–2151
16. Yang F, Jin S, Li Z, Ding S, Ma X (2017) A new error compensation model for machining process based on differential motion vectors. Int J Adv Manuf Technol 93:2943–2954
17. Paris H, Peigne G, Mayer R (2004) Surface shape prediction in high speed milling. Int J Mach Tools Manuf 44:1567–1576

18. Paris H, Peigné G, Brissaud D (2003) A model of milled surface generation for time domain simulation of high-speed cutting. Proc Inst Mech Eng Part B-J Eng Manuf 217:919–930
19. Lavernhe S, Tournier C, Lartigue C (2008) Kinematical performance prediction in multi-axis machining for process planning optimization. Int J Adv Manuf Technol 37:534–544
20. Honeycutt A, Schmitz TL (2017) A study of milling surface quality during period-2 bifurcations. Procedia Manuf 10:183–193
21. Dépincé P, Hascoët J (2006) Active integration of tool deflection effects in end milling. Part 1. Prediction of milled surfaces. Int J Mach Tools Manuf 46:937–944
22. Pimenov DY (2013) Geometric model of height of microroughness on machined surface taking into account wear of face mill teeth. J Frict Wear 34:290–293
23. Lavernhe S, Quinsat Y, Lartigue C (2010) Model for the prediction of 3D surface topography in 5-axis milling. Int J Adv Manuf Technol 51:915–924
24. Quinsat Y, Lavernhe S, Lartigue C (2011) Characterization of 3D surface topography in 5-axis milling. Wear 271:590–595
25. Zhang W, Tan G, Wan M, Gao T, Bassir DH (2008) A new algorithm for the numerical simulation of machined surface topography in multiaxis ball-end milling. J Manuf Sci Eng-Trans ASME 130: 11003
26. Omar OEEK, El-Wardany T, Ng E, Elbestawi MA (2007) An improved cutting force and surface topography prediction model in end milling. Int J Mach Tools Manuf 47:1263–1275
27. Song G, Li J, Sun J (2013) Approach for modeling accurate undeformed chip thickness in milling operation. Int J Adv Manuf Technol 68:1429–1439
28. Yang D, Liu Z (2015) Surface plastic deformation and surface topography prediction in peripheral milling with variable pitch end mill. Int J Mach Tools Manuf 91:43–53
29. Dong Z, Jiao L, Wang X, Liang Z, Liu Z, Yi J (2016) FEA-based prediction of machined surface errors for dynamic fixture-workpiece system during milling process. Int J Adv Manuf Technol 85:299–315
30. Felhő C, Karpuschewski B, Kundrák J (2015) Surface roughness modelling in face milling. Procedia CIRP 31:136–141
31. Lu Y, Ding Y, Zhu L (2017) Dynamics and stability prediction of five-axis flat-end milling. J Manuf Sci Eng-Trans ASME 139: 61015
32. Qu S, Zhao J, Wang T, Tian F (2015) Improved method to predict cutting force in end milling considering cutting process dynamics. Int J Adv Manuf Technol 78:1501–1510